Electrochimica Acta 91 (2013) 337–343

Contents lists available at SciVerse ScienceDirect

Electrochimica Acta

journal homepage: www.elsevier.com/locate/electacta

Sinter-free transferring of anodized TiO_2 nanotube-array onto a flexible and transparent sheet for dye-sensitized solar cells

Yu-Yen Kuo [a], Chao-Hsin Chien [a,b,*]

[a] Department of Electronics Engineering, National Chiao Tung University, 1001 Tahsueh Road, Hsinchu 30010, Taiwan
[b] National Nano Device Laboratories, 1 Prosperity Road I, Hsinchu 30050, Taiwan

ARTICLE INFO

Article history:
Received 25 October 2012
Received in revised form 1 January 2013
Accepted 1 January 2013
Available online 8 January 2013

Keywords:
Dye-sensitized solar cell
TiO_2 nanotube-array
Anodization
Flexible
Hydrothermal

ABSTRACT

A sinter-free method to transfer anodized TiO_2 nanotube-arrays to a polyethylene terephthalate (PET) sheet is proposed. Since the anodized nanotube-array was crystallized independently before transferring to the PET, the internal charge transport resistance and the charge recombination rate are unchanged for the nanotubes on the PET sheet, and no high temperature sintering process is required. With hydrothermal treatment, the dye sensitized solar cell fabricated utilizing a low temperature bonded nanotube/PET as a photoelectrode exhibits a power conversion efficiency of 5.41%, which is only 0.87% lower than the power conversion efficiency of the solar cell using nanotubes bonded on a conductive glass through high temperature processes.

1. Introduction

The greatly increased demand for energy over the past few decades has accelerated the need for research on renewable energy technologies. Among the various types of renewable energy, harvesting solar energy is one of the most promising solutions for a dispersed and abundant energy source. Although traditional semiconductor *p–n* junctions have demonstrated high solar energy harvesting efficiency, this approach is not suitable for terrestrial applications of solar energy collection because of the expensive materials required. To find a low cost solution for photovoltaics, many efforts have been focused on new types of solar cells composed of low cost materials. TiO_2, as an earth abundant, low cost and nontoxic material that has been widely researched in different applications such as: photocatalysis, gas-sensing and photoelectrolysis, and more recently nanostructured TiO_2 applications which have attracted increasing attention for potential applications in solar energy conversion [1–5].

As a highly efficient photoelectrode used in dye-sensitized solar cells (DSSC), TiO_2 nanoparticles are coated on a conductive glass to provide a large surface area for dye adsorption [6]. Optimized nanoparticle structures of DSSCs have reached an energy conversion efficiency of over 11% [7], and many researchers have fabricated DSSCs on a plastic substrate as a method to create low cost, light weight and flexible devices [8–11]. When fabricating the TiO_2 nanoparticle on a plastic substrate, high temperature sintering for the nanoparticles is not feasible due to the nature of plastics [12,13]. However, low temperature sintering will heavily degrade the charge collection efficiency of the TiO_2 nanoparticle and lower the photovoltaic performance of plastic DSSCs [14]. To enhance the charge collection ability of the TiO_2 nanopartilces on a plastic substrate, high pressure pressing, surface coating, chemical sintering and alternative depositions such as electrophoretic methods have been examined [15–20], but the enhancement is finite, and a more efficient photoelectrode on the plastic sheet remains a challenging issue.

In contrast to randomly organized nanoparticles, one-dimensionally oriented nanostructures, such as nanorods, nanowires, and nanotubes have also been studied to enhance the charge collection efficiency of DSSCs [21–24]. Among the various one-dimensional nanostructures, TiO_2 nanotube-arrays fabricated by anodization have exhibited many favorable characteristics as photoelectrodes of DSSC [25,26]. The as-anodized nanotube-array was on a titanium foil, a flexible DSSC can be fabricated directly using the as-anodized nanotube-array as the photoelectrode [27]. However, in such a configuration the DSSC needs to be back-side illuminated, which is a more unfavorable operating mode for DSSCs [28]. On the other hand, because of the feature of the compact connection among the anodized nanotubes, the nanotube-array can be detached from the titanium foil to

* Corresponding author at: Department of Electronics Engineering, National Chiao Tung University, 1001 Tahsueh Road, Hsinchu 30010, Taiwan. Tel.: +886 3 5712121x54252; fax: +886 3 5724361.
E-mail address: chchien@faculty.nctu.edu.tw (C.-H. Chien).

0013-4686/$ – see front matter © 2013 Elsevier Ltd. All rights reserved.
http://dx.doi.org/10.1016/j.electacta.2013.01.002

become a free-standing membrane and thus can be transferred to transparent substrates for the front-side incident DSSCs [29,30]. Although an energy conversion efficiency of over 8% by transferring the nanotube-array to a conductive glass have been reported [31–33], there have been very few studies on the fabrication of the nanotube-array on the plastic substrate. Anodization of a Ti layer deposited on a plastic sheet resulted into amorphous and short nanotubes, even with 350 °C annealing the performance of the DSSC is still limited [34,35]. On the other hand, when additional TiO_2 nanoparticles are introduced to bond the nanotube-array, the larger electrical resistance within the bonding layer using low temperature sintering could heavily lower the resulting charge collection of the nanotubes [36].

Instead of the intermediate TiO_2 bonding layer, we applied a more facile method to transfer the nanotube-array onto the plastic substrate. Using a well fabricated free-standing nanotube-array, we directly deposited an indium tin oxide (ITO) layer on top of the closed ends of the nanotubes. The ITO/nanotube membrane was bonded to an arbitrary substrate without applying high temperature processes. By transferring the nanotubes (NT) onto a polyethylene terephthalate (PET) sheet as a nanotube/PET (NT/PET) photoelectrode, the power conversion efficiency of the NT/PET DSSC was 5.41%. The impedance spectroscopy showed the internal electrical characteristics, including charge recombination rate, charge transport resistance and chemical capacitance of the NT/PET cell were similar to high temperature sintered nanotube DSSC on a conductive glass. These results indicated an efficient charge collection of the nanotube-array was achieved even without high temperature bonding processes.

2. Experimental methods

2.1. Preparation of TiO_2 nanotube-array

The TiO_2 nanotube-array was fabricated by anodization at constant voltage in a two electrode configuration. A bias of 50 V DC was applied to 0.25 mm Ti foil for 2 h with Pt serving as the counter electrode. The anodization was carried out in an electrolyte containing 0.3 wt% NH_4F and 2 vol% H_2O in ethylene glycol, and the reaction temperature was controlled at 40 °C by a temperature static tank. The length and the pore size of the anodized nanotube-array were identified to be 19 μm and 95 nm on average using a field emission scanning electron microscopy (FESEM, Hitachi-S4700). After the anodization, the nanotube-array was crystallized at 480 °C for 3 h under air flow, and CHF_3/CF_4 plasma was applied to the surface of the nanotube-array to clean the top ends of the nanotubes. For detachment of the crystallized nanotube-array from the Ti foil, anodization was applied again; the configuration, the electrolyte composition and the applied bias were all the same as the first anodization except the period was 1 h. Then, the crystallized nanotube-array was detached from the Ti foil by immersing the secondly anodized sample into 1 M hydrochloric acid.

2.2. Fabrication of NT/PET photoelectrode and the DSSC

Indium tin oxide (ITO, 5% SnO and 95% In_2O_3) of 400 nm was deposited onto the closed ends of the detached nanotube-array membrane by e-beam evaporation or by sputtering methods. For both methods the deposition rate was controlled to be approximately 1 Å s^{-1}. The e-beam evaporated sample was then annealed at 500 °C in N_2 ambient for 10 min for crystallization of the ITO layer. The transmittance and the sheet resistance of the deposited ITO layer were measured by UV–Vis spectroscopy and a four point probe respectively. The crystalline analyses of the ITO/nanotube composite membrane was performed by grazing incidence X-ray diffraction (GIXRD) using a PANalytical X'Pert Pro diffractometer with Cu Kα radiation.

To transfer the ITO deposited nanotubes to a plastic sheet, polydimethylsilane (PDMS, sylgard® 184) was spin coated onto a PET substrate. This was followed by stamping PDMS coated PET sheet onto the ITO deposited side of the nanotube-array, and then the nanotube-array was bonded to the PET after baking the PET sheet at 120 °C for 1 h. Finally, Ag was e-beam deposited into a small hole preserved on the PET sheet to make external contact to the ITO layer of the bounded nanotube-array, and then the hole was sealed by UV paste.

Next, the NT/PET electrode was immersed into a dye solution of 0.3 mM N719 (bis(tetrabutylammonium)[cis-di(thiocyanato)-bis(2,2′-bipyridul-4-carboxylate-4′-carboxylic acid)-ruthenium(II)]) in anhydrous ethanol for 18 h for dye adsorption. To fabricate DSSC, Pt sputtered ITO glass (7 Ω $\square^{-1}$) was used as the counter electrode to facilitate encapsulation. Between the NT/PET photoelectrode and the counter electrode was a spacer composed of a 60 μm thermoplastic film (SX1170-60, Solaronix), and an electrolyte containing 0.05 M I_2, 0.6 M 1-propyl-3-methylimidazolium iodide, 0.1 M LiI and 0.5 M 4-tertbutylpyridine in 3-methoxypropionitrile was injected into the space by capillary infiltration.

2.3. Characterization of the NT/PET DSSC

The photocurrent-voltage characteristic of the solar cell was characterized by a sourcemeter (Keithley 2400) under irradiation of 100 mW cm^{-2} provided by a solar simulator (Oriel 96000) equipped with an AM1.5G filter. The power density of the illumination was measured by a power meter (840-C, Newport). Electrochemical impedance spectroscopy (EIS) of the solar cell was measured by a potentiostat (EG&G 273a) equipped with a frequency response analyzer (EG&G 1025); AC signal with 10 mV amplitude was applied with a recorded frequency that ranged from 10^5 to 10^{-2} s^{-1}. The fitting of the impedance spectroscopy was implemented by Zview software.

3. Results and discussion

3.1. Material characteristics of the ITO/nanotube composite membrane

To fabricate the ITO/nanotube composite membrane, we examined different methods including e-beam evaporation and sputtering to deposit the ITO layer onto TiO_2 nanotube-array. The as-deposited ITO layer by e-beam evaporation was opaque due to a lower ratio of incorporated oxygen, and the sheet resistance of the as-deposited ITO was 57.2 Ω $\square^{-1}$. Conducting post annealing, the transmittance of the e-beam evaporated ITO layer improved to be over 80% in the visible wavelength region, and the sheet resistance decreased to 45.1 Ω $\square^{-1}$. On the other hand, the as-deposited ITO layer by sputtering showed higher than 85% transmittance increase at 530 nm and a sheet resistance 22 Ω $\square^{-1}$ so that post annealing was not necessary for this sample. Fig. 1 shows the FESEM images of the ITO/nanotube composite membranes deposited by e-beam or sputtering methods and their top-view and cross-sectional micromorphologies. Both the evaporated and sputtered ITO layer formed a continuous thin film on top of the closed ends of the compactly connected nanotube-array. However, the crystalline characteristic of the ITO layer significantly depended on the deposition method. Fig. 2 shows the X-ray diffraction results of the e-beam evaporated and sputtered ITO layers on a glass substrate or on the TiO_2 nanotube-array. There was no identifiable diffraction peaks for the as-deposited ITO by e-beam evaporation either on the glass

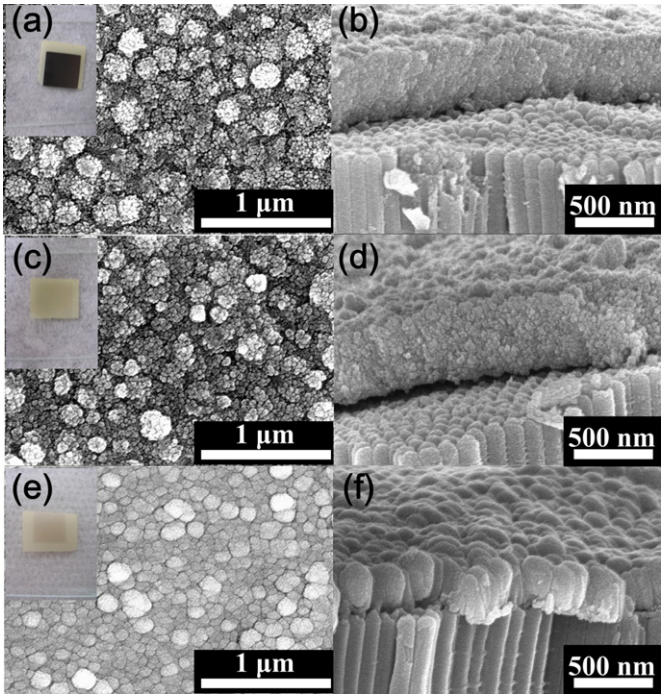

Fig. 1. Top-view and cross-sectional FESEM images of the ITO deposited onto the free-standing TiO_2 nanotube membrane by e-beam evaporation ((a) and (b)—as deposited, (c) and (d)—annealed) and by sputtering ((e) and (f)). Inserted in the top-view images are the photographs of the ITO/nanotube composite membrane.

or on the TiO_2 nanotubes. Hence, initially it was amorphous and the crystallinity was remarkably improved by applying post thermal annealing. In contrast, the ITO layer deposited by sputtering depicted good crystallinity even without post annealing. For both deposition methods the crystallinity of the ITO layer deposited on the TiO_2 nanotube-array was found to be inferior to those deposited on the bare glass. The crystallization of ITO was probably influenced by the curved surface of the closed ends of anodized nanotubes, which could limit the migration of the overlaying ITO.

3.2. Photovoltaic characteristics of the NT/PET DSSCs

To transfer the ITO/nanotube composite membrane onto the PET sheet to fabricate the NT/PET photoelectrode, polydimethylsilane (PDMS) was first spin coated on the PET sheet to serve as the

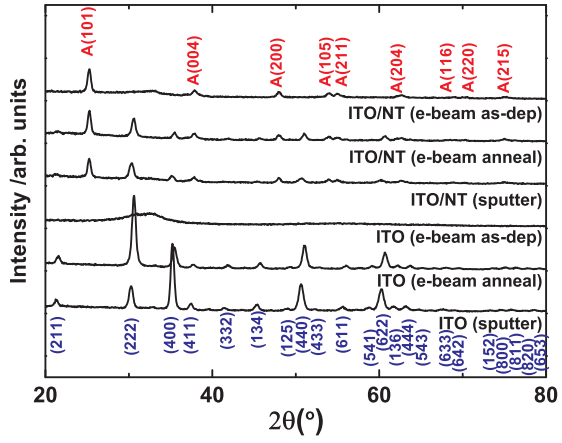

Fig. 2. XRD results of the ITO/nantube composite membrane of e-beam evaporation (without annealing) and sputtering methods. The peaks labeled by A in red color correspond to anatase phase, and the peaks labeled in blue refer to ITO facets. The XRD results of single ITO layer deposited on the bare glass by each method are also included.

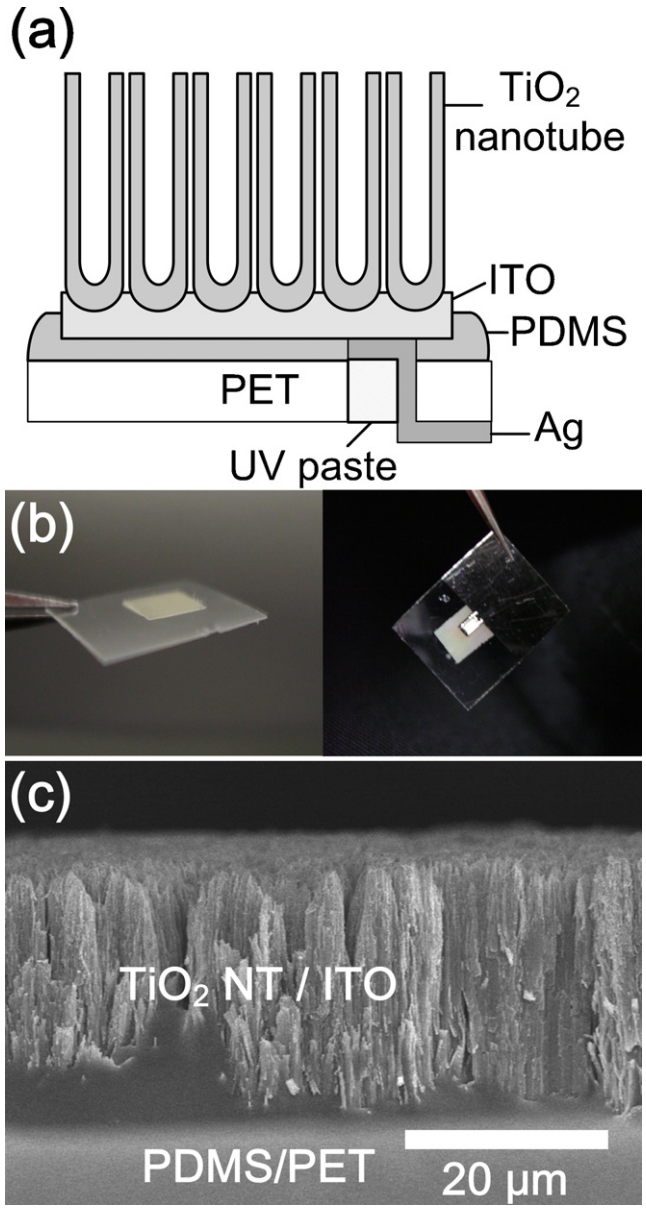

Fig. 3. (a) Structure of the NT/PET photoelectrode. (b) The front-side and back-side of the NT/PET photoelectrode. (c) The cross sectional FESEM image of the NT/PET photoelectrode.

bonding medium. Because of the fluidity of the PDMS, the ITO/nanotube membrane can be flatly and closely adhered to the flexible PET substrate after curing the PDMS layer, as shown in Fig. 3. Fig. 4 shows the photocurrent density–voltage (J–V) curves of DSSCs applying the NT/PET as the photoelectrode. The NT/PET DSSC with sputtered ITO showed a fill factor higher than that of NT/PET cell with e-beam evaporated ITO. This yielded a 0.3% difference in power conversion efficiency while the short-circuit photocurrent densities (J_{sc}) and open-circuit voltages (V_{oc}) of the NT/PET cells were similar using the different ITO deposition methods. The dependence of fill factor of NT/PET DSSCs on the ITO deposition method revealed that there was considerable recombination for electrons collected by the ITO layer. Since there are voids between the nanotubes, the electrolyte can infiltrate into these voids and make direct contact with the ITO layer in NT/PET DSSCs even though the nanotubes have closed bottom ends.

As shown in Fig. 4, NT/PET DSSC formed by directly transferring an as-detached nanotube-array to PET sheet had lower power conversion efficiency; there was a significant drop in V_{oc} and a greatly

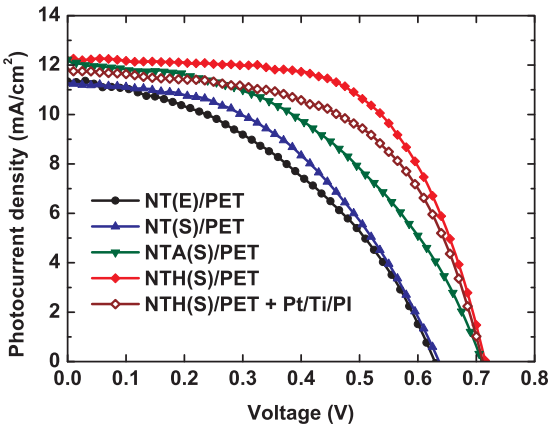

Fig. 4. Photocurrent density–voltage characteristics of the NT/PET DSSCs with ITO layer deposited on nanotubes by e-beam (NT(E)/PET), by sputtering (NT(S)/PET) and with nanotubes treated by post-annealing (NTA(S)/PET) or by a hydrothermal method (NTH(S)/PET), and the flexible NT/PET DSSC using hydrothermally treated nanotube with a flexible counter electrode of Pt/Ti sputtered on a polyimide sheet (NTH(S)/PET + Pt/Ti/PI). The measurement was carried out at 100 mW cm^{-2} illumination. The photocurrent densities of NT/PET cells were calculated by dividing the photocurrent by the active area of the cells, which was the total area of the nanotube subtracting the area of the Ag pad.

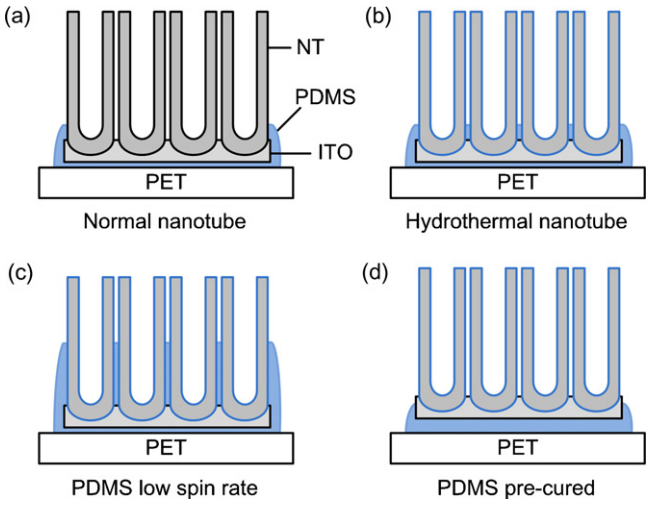

Fig. 5. Infiltration of PDMS when bonding ITO deposited TiO_2 nanotube-array to PET with (a) non-treated nanotubes, (b) hydrothermally treated nanotubes, (c) low spin coating rate for PDMS and (d) pre-cured PDMS.

decreased fill factor. When additional thermal annealing (450 °C, in air flow) was applied to the detached nanotube-array prior to the deposition of ITO layer, the V_{oc} of NT/PET DSSC was improved from 0.64 V to 0.71 V. We speculate that there might be chemical adsorbates on the surface of nanotubes or on the bottom layer left by the second anodization for detachment. The dipole induced by the adsorbate on the sidewall could shift the conduction band edge of TiO_2, and the dipole on the closed ends of nanotubes would induce overpotential at the interface between TiO_2 and ITO. Both would lead to the open-circuit voltage change. These adsorbates probably decompose or desorb with the help of thermal annealing and, thus result in the V_{oc} increase.

Although the V_{oc} of NT/PET DSSC could be improved to 0.71 V, however, the fill factor was barely influenced by the annealing. The fill factor of NT/PET DSSCs should be lowered by additional recombination processes within the NT/PET photoelectrode. By applying hydrothermal treatment in 15 ml de-ionized water for 2 h for the TiO_2 nanotubes used in the NT/PET DSSCs, we found the charge recombination could be efficiently inhibited. The details of the hydrothermal method were described in our previous report [37]. As shown in Fig. 4, with hydrothermal treatment the fill factor of the NT/PET DSSC increased to 0.61 and the power conversion efficiency of the solar cell increased to 5.41%.

The significant enhancement on fill factor of NT/PET DSSC by hydrothermal treatment is interesting. In our previous studies we identified the hydrothermal treatment could lead to increased hydroxyl groups on the surface of TiO_2 nanotubes, which decreased the recombination rate between the electrons on theTiO_2 conduction band and the holes in the electrolyte in DSSCs [37]. On the other hand, the increased surface hydroxyl groups would also promote the surface hydrophilicity of the TiO_2 nanotubes [38]. As a result, PDMS can more easily infiltrate into the voids between the hydrothermally treated nanotubes when the ITO deposited nanotube-array was transferred to PET. The infiltrated PDMS can isolate the ITO from the electrolyte in the NT/PET DSSC, shown as Fig. 5a and b, and for this reason electron–hole recombination between the ITO and electrolyte was efficiently suppressed, and thus the fill factor increased.

Table 1 summarizes the photovoltaic parameters of hydrothermally treated NT/PET DSSCs when different conditions were applied for PDMS coating; the performance of NT/PET DSSCs was found to be influenced by the spin rate and the pre-curing conditions for PDMS. This is because the PDMS coating conditions can change the infiltration ability of PDMS within the voids of nanotubes, as Fig. 5b–d show. In the experiment, we observed PDMS could easily infiltrate into and fill the voids of hydrothermally treated nanotubes when the spin rate was low, and dye adsorbed on the PDMS filled nanotubes decreased. The decreased dye load resulted in a decreased V_{oc} and a decreased J_{sc}. If the spin rate was increased or if the PDMS layer was cured before transferring the nanotubes the infiltration of PDMS could be suppressed. However, the fill factor of the NT/PET DSSC dropped when PDMS was cured over 10 min at 120 °C. We suggest this is because under such a condition ITO is less isolated from the electrolyte by PDMS, and charge recombination happens more frequently between the exposed ITO and electrolyte.

With the optimized NT/PET photoelectrode we applied Pt/Ti (50 nm/5 nm) sputtered polyimide sheet as the counter electrode to fabricate a flexible NT/PET DSSC. The counter electrode was baked at 300 °C before encapsulation. The measured *J–V* curve of the flexible NT/PET DSSC was included in Fig. 4. The J_{sc}, V_{oc} and power conversion efficiency were 11.79 mA cm^{-2}, 0.71 V and 4.77%, respectively. Because of the flexible cell structure electrolyte was found easily leak under irradiation. The performance should be able to be enhanced with an improved encapsulation.

3.3. Comparison of the characteristics of the low temperature NT/PET DSSC with the high temperature bonded nanotube/glass DSSC

Fig. 6 shows the measured EIS with corresponding best-fit curves of the hydrothermal NT/PET DSSC and a comparison with the impedance of the DSSC using nanotubes fabricated bonded on a conductive glass (SnO_2:F, 8 Ω □$^{-1}$). For the bonding of the nanotubes on a FTO glass, TiO_2 bonding sol containing titanium isopropoxide in ethanol and acetic acid was coated on the glass first, and after the nanotube-array was transferred onto the glass 450 °C sintering process was applied in atmospheric ambient. The photovoltaic parameters and the fitting parameters for the impedance spectroscopy were summarized in Table 2. The NT/PET DSSC and the NT/glass DSSC depicted distinct impedance characteristics at high frequencies. This resulted from the different structure of the photoelectrodes. For the NT/glass DSSC there were multiple impedance semicircles at high frequencies in the Nyquist plot.

Table 1
Photovoltaic parameters of hydrothermally treated NT/PET DSSCs with different coating conditions of PDMS layer.

Spin rate (rpm)	PDMS pre-curing	J_{sc} [mA cm^{-2}]	V_{oc} [V]	Fill factor	Power conversion efficiency [%]
1500	–	9.22 ± 0.10	0.69	0.55	3.47
2400	–	12.36 ± 0.10	0.72	0.61	5.41
2400	120 °C 10 min	10.75 ± 0.10	0.73	0.58	4.54
2400	120 °C 20 min	9.78 ± 0.07	0.72	0.54	3.81

The smaller semicircle at the highest frequencies near 10^5 s^{-1} was caused by the interfacial resistance r_i and capacitance c_i between the TiO_2 photoelectrode and the conductive glass whereas the second semicircle at 10^4 s^{-1} was dominated by charge transferring impedance c_p and r_p between the electrolyte and the Pt counter electrode [39]. The interfacial impedances r_i and c_i between the ITO and the nanotubes were larger than those between the conductive glass and the nanotubes since the NT/PET was prepared by a sinter-free method.

At frequencies of 10^2–10^3 s^{-1} the impedance was mostly influenced by the transport resistance R_w, which was also found to be different in NT/PET DSSC (4.1 Ω) and in NT/glass DSSC (11.2 Ω). The difference on R_w should be ascribed to the resistance of the bonding layer in NT/glass because the bonding layer was composed of titania with a grain size much smaller than the crystallite size of the nanotube. Similar effects on the impedance can be more obviously observed in the low temperature bonded NT/glass DSSCs, as reported by J. Luo et al. [36].

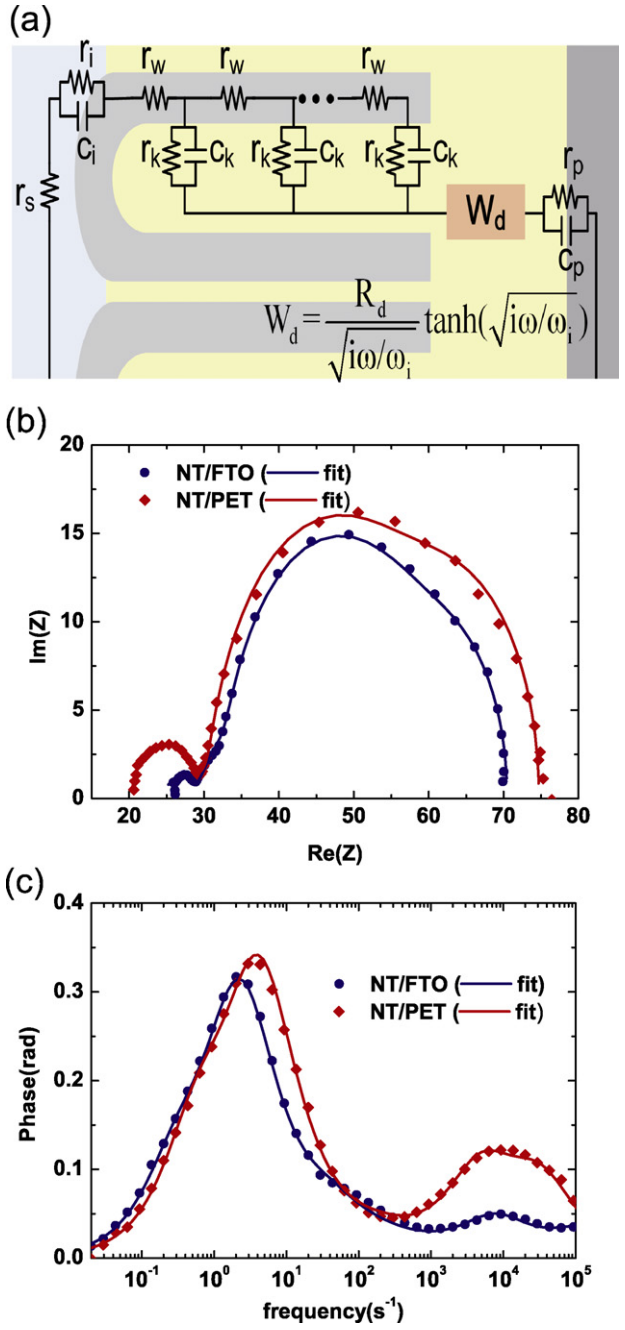

Fig. 6. (a) Impedance model considered in fitting the DSSCs at open-circuit conditions. W_d represents the finite length Warburg element. (b) Nyquist plots and the fitting curve of the NT/glass DSSC and the NT/PET DSSC. (c) Spectroscopy and the fitting curve of the phase of the impedance of the NT/glass DSSC and the NT/PET DSSC. The impedance was measured at irradiation of 100 mW cm^{-2} when the DSSC was biased at open-circuit voltage.

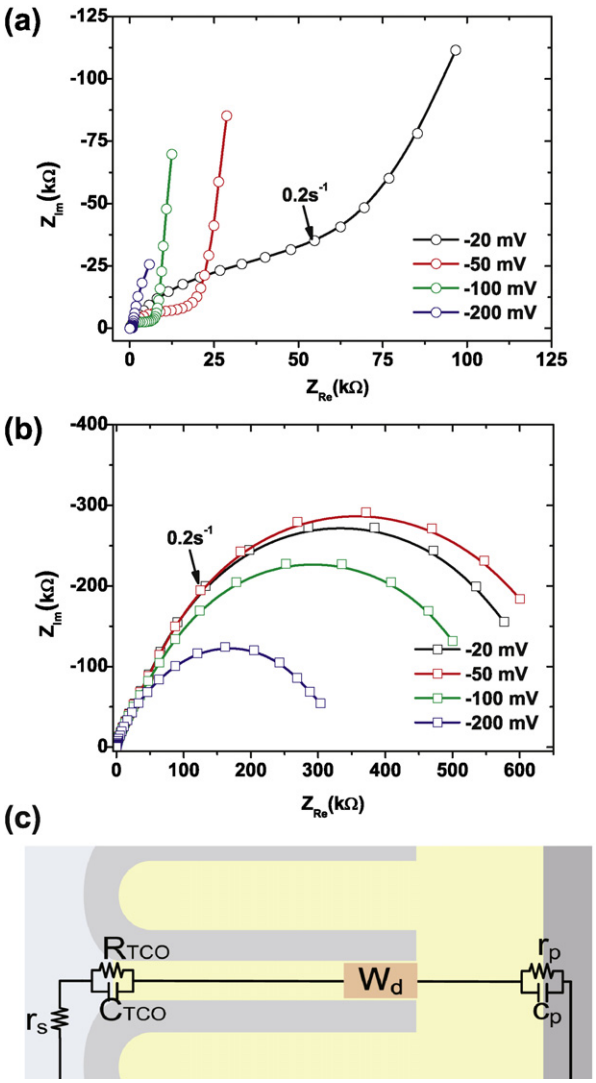

Fig. 7. (a) Nyquist plots of the NT/PET DSSC biased at low potentials in dark. (b) Nyquist plots of the NT/glass DSSC biased at low potentials in dark. (c) The charge transferring path of the DSSCs at low potentials in dark.

Table 2
The photovoltaic parameters and the impedance parameters of NT/PET DSSC and NT/glass DSSC. The parameters corresponded to the components in Fig. 3b. $r_w = R_w/L$, $r_k = R_k L$, $c_k = C_k/L$ whereas L was the thickness of the TiO_2 layer. The active area of the cells was 0.16 cm^2.

Photoelectrode	J_{sc} (mA cm^{-2})	V_{oc} (V)	FF	PCE (%)	$r_s(\Omega)$	$R_w(\Omega)$	$R_k(\Omega)$	$C_k(10^{-3}F)$	$R_d(\Omega)$	$\omega_d(s^{-1})$	$c_p(10^{-6}F)$	$r_p(\Omega)$	$c_i(10^{-7}F)$	$r_i(\Omega)$
NT/PET	12.36	0.72	0.61	5.41	20.3	4.1	23.4	2.3	21.7	1.43	7.5	4.7	16.0	3.2
NT/glass	12.98	0.70	0.69	6.28	25.9	11.2	24.1	3.9	14.4	0.71	9.9	2.2	8.7	1.5

At low frequencies of 10^1–10^{-2} s^{-1} the impedances of the NT/PET DSSC and the NT/glass DSSC were similarly dominated by charge transferring from the TiO_2 nanotube to the electrolyte and by ionic diffusion in the electrolyte [40]. Because of the additional electron recombination path from ITO to the electrolyte, the charge transferring rate $\omega_k = (R_k C_k)^{-1}$ for NT/PET DSSC was 19 s^{-1}, which was higher than 11 s^{-1} for NT/glass DSSC. The difference on ω_k should be the main reason for the lower fill factor and the lower conversion efficiency of the NT/PET DSSC than those of the NT/glass DSSC. On the other hand, the ionic diffusion rate ω_d was identified to be higher in NT/PET DSSC when the diffusion could be retarded within the bonding layer in NT/glass DSSC.

The charge transferring between the transparent conductive oxide (ITO for NT/PET; FTO for NT/glass) and the electrolyte that influenced the fill factor of the DSSCs was further investigated. Fig. 7a and b shows the Nyquist plots of the NT/PET and NT/glass DSSCs measured in dark at low DC potentials. At low potentials, the charge transferring between the conductive oxide and the electrolyte was dominant over the charge transferring between TiO_2 and the electrolyte [41], with the DSSC charge transferring path shown in Fig. 7c. Since the interfacial resistance R_{TCO} was large in the NT/glass DSSC, the cell impedance was obviously dominated by this interfacial impedance. On the other hand, the charge transferring resistance between exposed ITO and the electrolyte in the NT/PET DSSC was much smaller, and thus the impedances were then dominated by the Warburg diffusion element at frequencies lower than ca. 0.2 s^{-1}.

4. Conclusion

With the previously deposited ITO layer, the ITO/nanotube composite membrane can be transferred to any substrate, e.g. decomposable materials, at low temperature. As seen in the photoelectrode in the DSSC, the charge collection of the low temperature bonded NT/PET was highly efficient. The conductance and the ionic diffusion rate in the NT/PET were identified to be higher than the NT/glass using an intermediate bonding layer. A critical issue for the NT/PET DSSC was the recombination between the deposited ITO and the electrolyte. We found applying hydrothermal treatment to nanotubes and using proper conditions for bonding could efficiently inhibit the recombination and improve the performance of the NT/PET DSSC. According to this research, depositing a chemically resistant transparent conductive layer onto the nanotube-array is expected to further enhance the performance of the NT/PET DSSCs.

Acknowledgements

We are grateful to the National Nano Device Laboratory for supporting XRD measurements, and acknowledge Nano Facility Center at National Chiao Tung University for the FESEM and the e-beam evaporation system. Especially, we would like to thank Dr. J.-M. Shieh, Dr. C.-H. Shen and Mr. T.-T. Wu in the National Nano Device Laboratory for assistance in ITO sputtering.

References

[1] A.L. Linsebigler, G. Lu, J.T. Yates Jr., Photocatalysis on TiO_2 Surfaces: principles, mechanisms, and selected results, Chemical Reviews 95 (1995) 735.
[2] C. Wang, L. Yin, L. Zhang, Y. Qi, N. Lun, N. Liu, Large scale synthesis and gas-sensing properties of anatase TiO_2 three-dimensional hierarchical nanostructures, Langmuir 26 (2010) 12841.
[3] S.K. Mohapatra, K.S. Raja, V.K. Mahajan, M. Misra, Efficient photoelectrolysis of water using TiO_2 nanotube arrays by minimizing recombination losses with organic additives, Journal of Physical Chemistry C 112 (2008) 11007.
[4] Y.Y. Lin, T.H. Chu, S.S. Li, C.H. Chuang, C.H. Chang, W.F. Su, C.P. Chang, M.W. Chu, C.W. Chen, Interfacial nanostructuring on the performance of polymer/TiO_2 nanorod bulk heterojunction solar cells, Journal of the American Chemical Society 131 (2009) 3644.
[5] P.V. Kamat, TiO_2 nanostructures: recent physical chemistry advances, Journal of Physical Chemistry C 116 (2012) 11849.
[6] B. O'Regan, M. Grätzel, A low-cost, high-efficiency solar cell based on dye-sensitized colloidal TiO_2 films, Nature 353 (1991) 737.
[7] M.A. Green, K. Emery, Y. Hishikawa, W. Warta, E.D. Dunlop, Solar cell efficiency tables (version 39), Progress in Photovoltaics: Research and Applications 20 (2012) 12.
[8] F. Pichot, J.R. Pitts, B.A. Gregg, Low-temperature sintering of TiO2 colloids: application to flexible dye-sensitized solar cells, Langmuir 16 (2000) 5626.
[9] Y. Kijitori, M. Ikegami, T. Miyasaka, Highly efficient plastic dye-sensitized photoelectrodes prepared by low-temperature binder-free coating of mesoscopic titania pastes, Chemistry Letters 36 (2007) 190.
[10] H.C. Weerasinghe, P.M. Sirimanne, G.V. Franks, G.P. Simon, Y.B. Cheng, Low temperature chemically sintered nano-crystalline TiO_2 electrodes for flexible dye-sensitized solar cells, Journal of Photochemistry and Photobiology A 213 (2010) 30.
[11] T. Yamaguchi, N. Tobe, D. Matsumoto, T. Nagai, H. Arakawa, Highly efficient plastic-substrate dye-sensitized solar cells with validated conversion efficiency of 7.6%, Solar Energy Materials and Solar Cells 94 (2010) 812.
[12] Y. Wang, J.H. Wu, Z. Lan, Y.M. Xiao, Q.B. Li, F.G. Peng, J.N. Lin, M.L. Huang, Preparation of porous nanoparticle TiO_2 films for flexible dye-sensitized solar cells, Chinese Science Bulletin 56 (2011) 2649.
[13] M.G. Kang, N.G. Park, K.S. Ryu, S.H. Chang, K.J. Kim, A 4.2% efficient flexible dye-sensitized TiO_2 solar cells using stainless steel substrate, Solar Energy Materials and Solar Cells 90 (2006) 574.
[14] J.H. Tinguely, R. Solarska, A. Braun, T. Graule, Low-temperature roll-to-roll coating procedure of dye-sensitized solar cell photoelectrodes on flexible polymer-based substrates, Semiconductor Science and Technology 26 (2011) 045007.
[15] M. Dürr, A. Schmid, M. Obermaier, S. Rosselli, A. Yasuda, G. Nelles, Low-temperature fabrication of dye-sensitizedsolar cellsby transfer of composite porous layers, Nature Materials 4 (2005) 607.
[16] S.S. Kim, J.H. Yum, Y.E. Sung, Flexible dye-sensitized solar cells using ZnO coated TiO_2 nanoparticles, Journal of Photochemistry and Photobiology A: Chemistry 171 (2005) 269.
[17] N.G. Park, K.M. Kim, M.G. Kang, K.S. Ryu, S.H. Chang, Y.J. Shin, Chemical sintering of nanoparticles: a methodology for low-temperature fabrication of dye-sensitized TiO_2 Films, Advanced Materials 17 (2005) 2349.
[18] J.H. Yum, S.S. Kim, D.Y. Kim, Y.E. Sung, Electrophoretically deposited TiO_2 photo-electrodes for use in flexible dye-sensitized solar cells, Journal of Photochemistry and Photobiology A: Chemistry 173 (2005) 1.
[19] X. Yin, Z. Xue, L. Wang, Y. Cheng, B. Liu, High-performance plastic dye-sensitized solar cells based on low-cost commercial P25 TiO_2 and organic dye, ACS Applied Materials & Interfaces 4 (2012) 1709.
[20] W.H. Chiu, K.M. Lee, W.F. Hsieh, High efficiency flexible dye-sensitized solar cells by multiple electrophoretic depositions, Journal of Power Sources 196 (2011) 3683.
[21] J.J. Kim, K.S. Kim, G.Y. Jung, Fabrication of flexible dye-sensitised solar cells with photoanodes composed of periodically aligned single crystalline vertical ZnO NRs by utilising a direct metal transfer method, Journal of Materials Chemistry 21 (2011) 7730.
[22] J. Jiu, S. Isoda, F. Wang, M. Adachi, Dye-sensitized solar cells based on a single-crystalline TiO_2 nanorod film, Journal of Physical Chemistry B 110 (2006) 2087.
[23] M. Law, L.E. Greene, J.C. Johnson, R. Saykally, P. Yang, Nanowire dye-sensitized solar cells, Nature Materials 4 (2009) 455.
[24] G.K. Mor, K. Shankar, M. Paulose, O.K. Varghese, C.A. Grimes, Use of highly-ordered TiO_2 Nanotube arrays in dye-sensitized solar cells, Nano Letters 6 (2006) 215.
[25] K. Zhu, N.R. Neale, A. Miedaner, A.J. Frank, Enhanced charge-collection efficiencies and light scattering in dye-sensitized solar cells using oriented TiO_2 Nanotubes arrays, Nano Letters 7 (2007) 69.
[26] J. Wang, Z. Lin, Dye-sensitized TiO_2 Nanotube solar cells with markedly enhanced performance via rational surface engineering, Chemistry of Materials 22 (2010) 579.

[27] D. Kuang, J. Brillet, P. Chen, M. Takata, S. Uchida, H. Miura, K. Sumioka, S.M. Zakeeruddin, M. Grätzel, Application of highly ordered TiO_2 nanotube arrays in flexible dye-sensitized solar cells, ACS Nano 2 (2008) 1113.
[28] P.T. Hsiao, Y.J. Liou, H. Teng, Electron transport patterns in TiO_2 nanotube arrays based dye-sensitized solar cells under frontside and backside illuminations, Journal of Physical Chemistry C 115 (2011) 15018.
[29] C.T. Yip, M. Guo, H. Huang, L. Zhou, Y. Wang, C. Huang, Open-ended TiO_2 nanotubes formed by two-step anodization and their application in dye-sensitized solar cells, Nanoscale 4 (2012) 448.
[30] Q. Chen, D. Xu, Noncurling, and free-standing crystallized TiO_2 Nanotube arrays for dye-sensitized solar cells, Journal of Physical Chemistry C 113 (2009) 6310.
[31] J. Choi, S.H. Park, Y.S. Kwon, J. Lim, I.Y. Song, T. Park, Facile fabrication of aligned doubly open-ended TiO_2 nanotubes, via a selective etching process, for use in front-illuminated dye-sensitized solar cells, Chemical Communications 48 (2012) 8748.
[32] C.J. Lin, W.Y. Yu, S.H. Chien, Transparent electrodes of ordered opened-end TiO_2-nanotube arrays for highly efficient dye-sensitized solar cells, Journal of Materials Chemistry 20 (2010) 1073.
[33] B.X. Lei, J.Y. Liao, R. Zhang, J. Wang, C.Y. Su, D.B. Kuang, Ordered crystalline TiO_2 nanotube arrays on transparent FTO glass for efficient dye-sensitized solar cells, Journal of Physical Chemistry C 114 (2010) 15228.
[34] V. Galstyan, A. Vomiero, E. Comini, G. Faglia, G. Sberveglieri, TiO_2 nanotubular aand nanoporous arrays by electrochemical anodization on different substrates, RSC Advances 1 (2011) 1038.
[35] A. Vomiero, V. Galstyan, A. Braga, I. Concina, M. Brisotto, E. Bontempi, G. Sberveglieri, Flexible dye sensitized solar cells using TiO_2 nanotubes, Energy & Environmental Science 4 (2011) 3408.
[36] J. Luo, L. Gao, J. Sun, Y. Liu, A bilayer structure of a titania nanoparticle/highly-ordered nanotube array for low-temperature dye-sensitized solar cells, RSC Advances 2 (2012) 1884.
[37] Y.Y. Kuo, T.H. Li, J.N. Yao, C.Y. Lin, C.H. Chien, Hydrothermal crystallization and modification of surface hydroxylgroups of anodized TiO_2 nanotube-arrays for more efficient photoenergy conversion, Electrochimica Acta 78 (2012) 236.
[38] M. Miyauchi, H. Tokudome, Super-hydrophilic and transparent thin films of TiO_2 nanotube arrays by a hydrothermal reaction, Journal of Materials Chemistry 17 (2007) 2095.
[39] T. Hoshikawa, M. Yamada, R. Kikuchi, K. Eguchi, Impedance analysis of internal resistance affecting the photoelectrochemical performance of dye-sensitized solar cells, Journal of the Electrochemical Society 152 (2005) E68.
[40] M. Adachi, M. Sakamoto, J. Jiu, Y. Ogata, S. Isoda, Determination of parameters of electron transport in dye-sensitized solar cells using electrochemical impedance spectroscopy, Journal of Physical Chemistry B 110 (2006) 13872.
[41] F. Fabregat-Santiago, J. Bisquert, G. Garcia-Belmonte, G. Boschloo, A. Hagfeldt, Influence of electrolyte in transport and recombination in dye-sensitized solar cells studied by impedance spectroscopy, Solar Energy Materials and Solar Cells 87 (2005) 117.